Separation of lattice structural and electronic effects on physical properties with nanotechnology

S. Li · Y. Y. Tay · C. Q. Sun

Abstract Physical properties of electronic and photonic materials can be significantly modified by partial altervalent/aliovalent chemical substitutes. The modification arises from the subtle interplay between the competing/cooperating effects of the electron and lattice structural variations, which are induced by the different charge and atomic radii of the substituents. To understand these effects, it is necessary to isolate the electronic and crystallographic contributions to the particular physical property to arrive at a fundamental understanding of the underlying dominant mechanism. Intrinsic properties amplified nanomaterials/nanoparticles is a newly developed technique which can experimentally discriminate lattice structural effects from electronic contributions to physical properties by exploiting the nanosize dependence of lattice structure to modify the structural parameters without resorting to chemical doping. In this work, we demonstrate a separation of structural and electronic effects on superconducting critical temperatures (T_c) of MgB_2 and $YBa_2Cu_3O_{7-x}$, and also on emission behavior of ZnO. The results show that the superconductivity of MgB_2 is extremely sensitive to lattice parameter variation while T_c of $YBa_2Cu_3O_{7-x}$ is more sensitive to electronic structure. The effects of the lattice and electronic structures on the emission behavior of ZnO are complex and the structural variations make different contributions to the behavior in the particular conditions.

Keywords Lattice · Nanotechnology · Doping · XRD refinement

1 Introduction

Partial altervalent/aliovalent chemical substitutions for cation or anion are widely used to modify the physical properties of semiconductors, electronic ceramics and photonic materials etc. by (1) changing the Fermi-level density-of-states with minimum disruption of the electronic network, and (2) altering the lattice parameters, thus achieving the desired properties for practical applications. However, such substitutions always raise a subtle interplay between the competing/cooperating effects of the electron and lattice structural variations, which are induced by the different charge and atomic radii of the substituents. Sometimes, it is difficult to understand the individual contribution from these variations, leading to seeking new materials with doping technology blindly. A typical example is: a number of elements have been attempted to add into MgB_2 to increase the critical transition temperature (T_c) but most of the substitutions studied to date depress T_c and at higher replacements completely suppress the superconductivity of MgB_2 [1–6]. This behavior is different from Cu oxide superconductors in which replacement of La by Y in La_2CuO_4 forms $YBa_2Cu_3O_{7-\delta}$ and raises T_c from 35 to 92 K. Therefore, to understand the fundamental mechanism of the dominant factors for the properties it is necessary to develop a technique to isolate the electronic and crystallographic contributions for study. It is generally true that the lattice constants of bulk materials are modified

S. Li (✉) · Y. Y. Tay
School of Materials Science and Engineering,
The University of New South Wales,
Sydney, NSW 2052, Australia
e-mail: sean.li@unsw.edu.au

C. Q. Sun
School of Electrical and Electronic Engineering,
Nanyang Technological University, Singapore
639798, Singapore

as crystal sizes approach nanoscales, resulting in bond length and angle variation, and in extreme cases, changes in atomic coordination numbers (CN). This intrinsic structural behavior of nanomaterial lattices allows the structural parameters of the materials to be modified without resorting to chemical doping. In this work, we report a newly developed technique which can experimentally discriminate lattice structural effects from electronic contributions to physical properties by exploiting the nanosize dependence of lattice structure.

2 Experiment

Hydrostatic pressure was used to vary the lattice parameters to investigate the lattice parameter effects on physical properties of the electronic materials [7]. However, pressure and temperature are intensive variables of a thermodynamic system, and any adjustment of these may result in phase changes that strongly influence the properties as evidenced by the appearance of superconductivity in Fe [8], UGe_2 [9], B, Li and Pt etc. at high hydrostatic pressure. Usually thought, the application of external pressure leads only to a limited compression of lattice parameters that is insufficient to cause changes in coordination number.

An alternative method to precisely modify lattice structural parameters, while avoiding possible complications induced by temperature and pressure, is by physical reduction of crystal size through ball-milling in tungsten carbide (WC) bowls purged with Ar. In this manner, highly reproducible size reduction could be achieved as a function of milling time. To determine lattice parameters including bond lengths and angles with high precision, Rietveld analysis was carried out using a fundamental parameter

procedure as implemented on TOPAS R (version 2.1). In addition, mechanical contamination from unreacted WC with less than 1 wt.% was detected in samples with the longest milling durations. Quantitative analysis showed that except for size variation and modulation of structural parameters, no other chemical reactions occurred during the milling process. High-resolution transmission electron microscopy (HRTEM) was employed to verify the crystal sizes determined by XRD. Magnetic moment as a function of temperature was measured in loose powder form with Oxford MagLab Systems by zero field cooling at 1 Oe and the photoluminescence was determined by Rapid Photoluminescence Mapping System with an excitation wavelength of 325 nm.

3 Results and discussion

3.1 Lattice dependence of critical transition temperature of MgB_2

It is believed that the diminution and loss of superconductivity in most of doped MgB_2 arises from the subtle interplay between the competing/cooperating effects of the electronic and lattice structural variations. To understand the mechanism behind these depression and suppressions it is necessary to separate the lattice parameters from electron contribution to the superconductivity of MgB_2. Figure 1 plots magnetic moments as a function of temperature for the as-prepared nano-crystalline MgB_2 materials. There is a size dependence of T_c (the temperature of transition onset) such that is invariant for crystal sizes from 64.1 to 11.8 nm, but dramatically decreases to 13.2 K for the crystals below 11.8 nm. For the smallest crystals (2.5 nm) superconducti-

Fig. 1 Magnetic moments as a function of temperature showing size dependence of superconducting transition temperature of MgB_2. T_c is invariant with the reduction of crystal sizes from 64.1 to 11.8 nm, but dramatically decreases to 13.2 K as the crystal size is further reduced to 4 nm. For the smallest crystals of MgB_2 (2.5 nm) superconductivity is completely lost
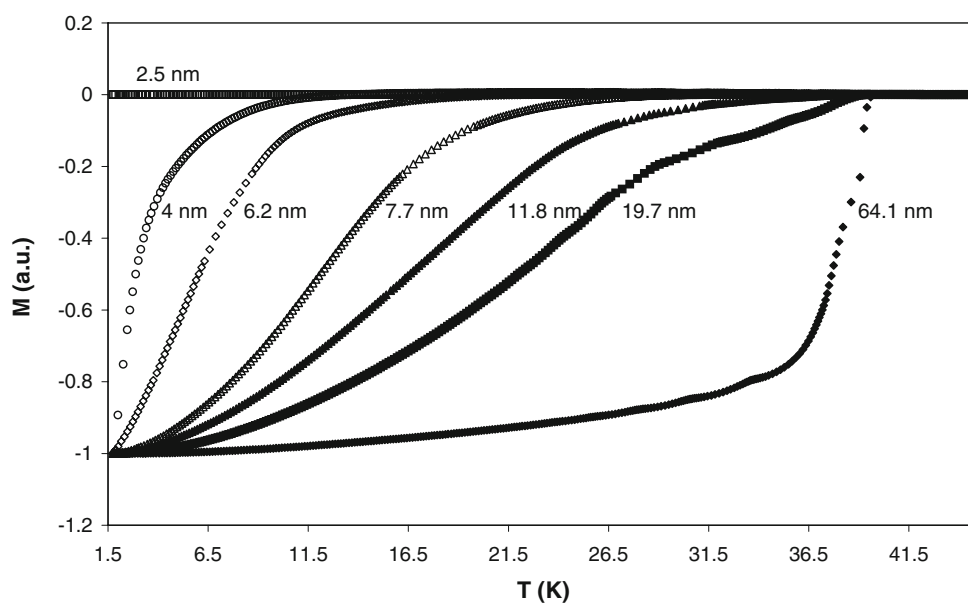
vity is completely lost. For the as-prepared MgB_2 materials, structural parameters as a function of crystal size are listed in Table 1 and plotted in Fig. 2, respectively. The geometry of the structural parameters requires that B-Mg-B and Mg-B-Mg bond angles change cooperatively. From Fig. 2(a) and (b), it can be clearly seen that the trends of cell volume, c-axis, Mg–B bond length, B-Mg-B and Mg-B-Mg bond angles do not correlate with T_c, suggesting these factors are not directly influencing the transition temperature. The P622 symmetry of MgB_2 constrains the Mg-Mg-Mg and B-B-B angles to 120°, thereby maintaining perfect Mg 3^6 and B 6^3 subnets regardless of crystal size, so these features cannot be responsible for the depression of T_c. However, Mg–Mg and B–B bond lengths trend with T_c, which is almost independent of crystal size from 64.1 to 11.8 nm, but decreases dramatically below 11.8 nm [Fig. 2(c)]. This implies that Mg–Mg and B–B bonds are the critical structural parameters that correlate with T_c. These results, and the trend of the Mg–Mg bond length effect on T_c, are in agreement with the results obtained by hydrostatic pressure experiments although the effect of hydrostatic pressure was weaker [7].

It is difficult to separate the individual contributions from Mg–Mg ($=a$) and B–B $\left(= a/\sqrt{3}\right)$ bonds to T_c as they are geometrically linked to the a-parameter and independent of the c-axis. However, for the smallest crystals, the relative Bragg intensities can only be successfully matched during Rietveld refinement through the introduction of statistically distributed B-vacancies, with the refined value falling from 1 to 2/3. In other words, the average coordination of Mg to B falls from 12 to 8, resulting in the loss of superconductivity. As expected from geometry, the Mg–Mg bond has similar nanosize dependence of relative variation percentage with B–B bond, but Mg retains full occupancy regardless the crystal size. It has been reported elsewhere that the contraction of Mg–Mg bonds will be limited due to the need to maintain a reasonable B–B distance [10]. Our results suggest that for small crystals (<4 nm) Mg–Mg bond shortening can be accommodated through the introduction of B vacancies. Therefore, the statistical occupation of the B-site allows Mg–Mg bond to contract further than might otherwise be possible, and this distance is the primary determinant of T_c in MgB_2. This result is also in agreement with the theoretical prediction in 7 nm by "Bond order-length-strength correlation mechanism" [11].

T_c depression and suppression have also been observed in altervalent/aliovalent chemical substituted MgB_2 materials. T_c is depressed significantly with addition of Al in $Mg_{1-x}Al_xB_2$ and the superconductivity is lost at $x=0.4$ (Fig. 3) [1]. The association of Al substitution is subtle and complex, with physical properties determined by the interplay of both electron and lattice structures. In Mg_{1-x}

Table 1 Structural parameters as a function of crystal size in MgB_2.

| Size (nm)	T_c (K)	Cell volume (Å3)	a Axis (Mg–Mg) (Å) a	c Axis (Å) c	B–B bond (Å) $a/\sqrt{3}$	Mg–B bond (Å) $\left[(c/2)^2 + (a/\sqrt{3})^2\right]^{1/2}$	B–Mg–B angle (degree) $2\left\{\sin^{-1}\left[\left[(a/\sqrt{3})/2\right]/\left[\left[(c/2)^2+(a/\sqrt{3})^2\right]^{1/2}\right]\right]\right\}$	Mg–B–Mg angle (degree) $2\left\{\sin^{-1}\left[(a/2)/\left[\left[(c/2)^2+(a/\sqrt{3})^2\right]^{1/2}\right]\right]\right\}$
64.1	39.2	29.06	3.0864(2)	3.5226(2)	1.7819(1)	2.5055(1)	41.67	76.04
19.7	39.2	29.08	3.0866(4)	3.5452(6)	1.7821(2)	2.5062(3)	41.66	76.02
11.8	39.2	29.10	3.0867(6)	3.6266(10)	1.7821(2)	2.5070(4)	41.65	75.99
7.7	29.6	29.12	3.0863(8)	3.5299(13)	1.7819(3)	2.5080(5)	41.62	75.95
6.2	21.8	28.95	3.0746(12)	3.5363(20)	1.7751(5)	2.5055(8)	41.50	75.70
4	13.2	28.88	3.0735(14)	3.5303(24)	1.7745(6)	2.5029(10)	41.53	75.76
2.5	0	28.09	3.0505(27)	3.4853(44)	1.7612(11)	2.4776(19)	41.65	75.99
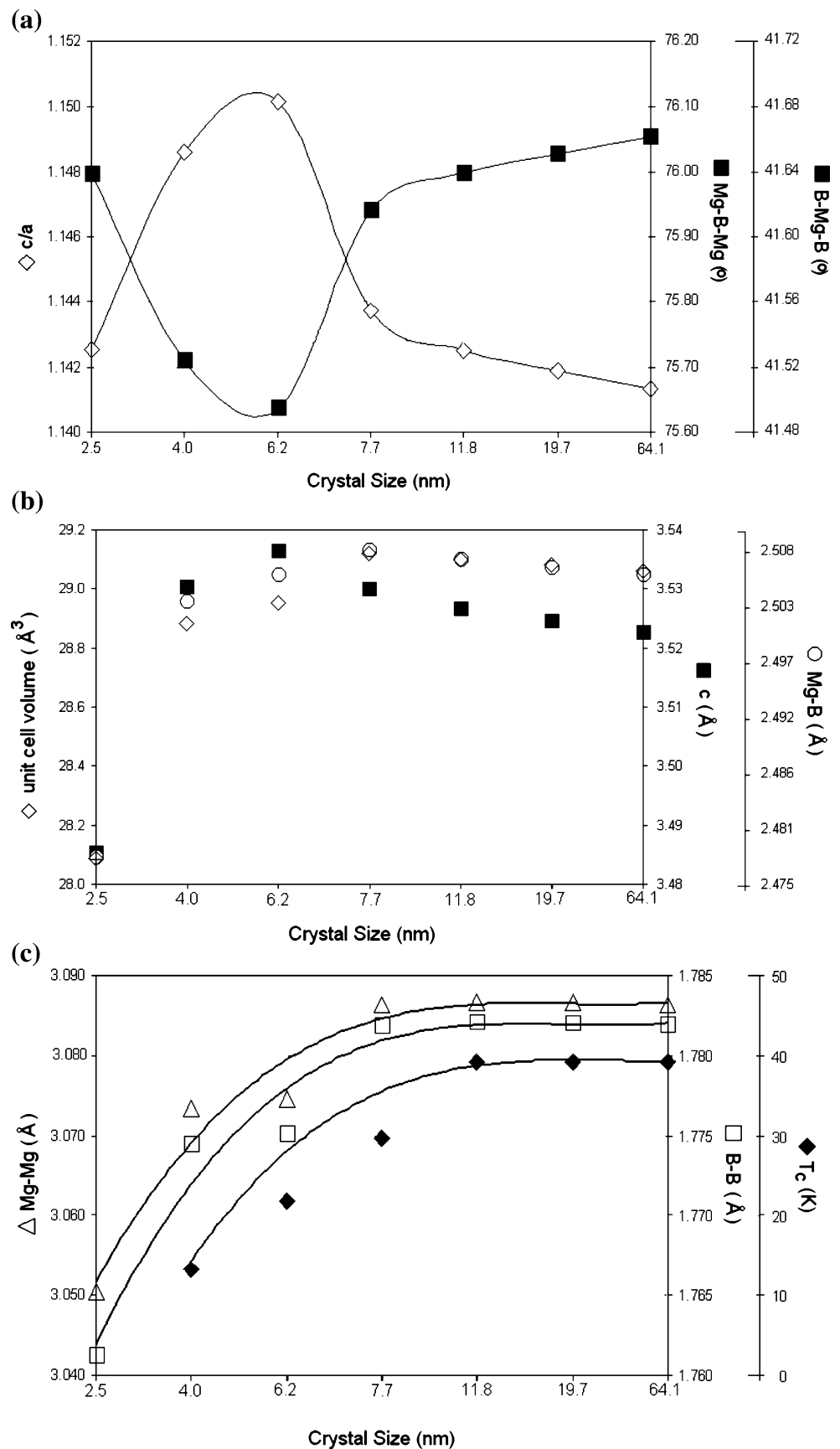
Fig. 3 Similar behaviors in Mg–Mg bond length dependence of T_c supporting the notion that the superconductivity of MgB_2 is highly sensitive to lattice structure and the Mg–Mg bond dominates the superconducting transition behavior
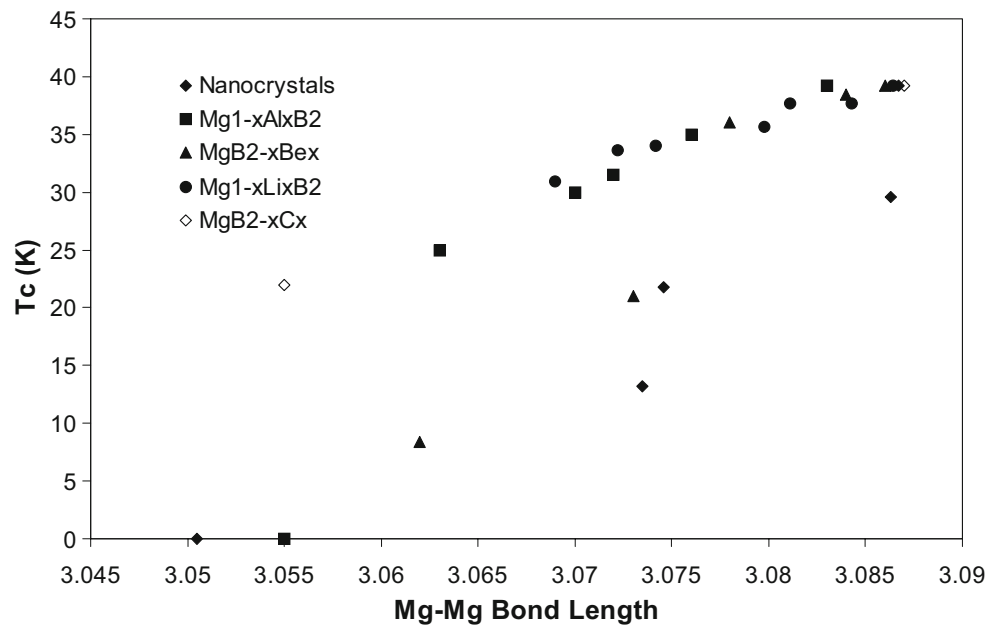
Al_xB_2, the a-axis (Mg–Mg bond) contracts from 3.083 to 3.055 Å, while the contraction of c-axis is from 3.526 to 3.367 Å, as x increases from 0 to 0.4 [2]. Although the variation of c-axis in $Mg_{0.6}Al_{0.4}B_2$ is greater than that in the nano-crystalline MgB_2 of 2.5 nm, the lengths of their Mg–Mg bonds are similar. This suggests that the loss of superconductivity in $Mg_{0.6}Al_{0.4}B_2$ may be a result of the Mg–Mg bond contraction caused by smaller Al. Except for the electron doping in $Mg_{1-x}Al_xB_2$, the hole doping with cation substitution of Li for Mg in $Mg_{1-x}Li_xB_2$ also depresses T_c [3] in a similar way as the contraction of Mg–Mg bond (Fig. 3). The significance of the Mg–Mg bond effects on T_c can also be found in MgB_2 where B is partially replaced by Be (hole doping) and C (electron doping). Although c-axis increases as Be increases from $x=0$–0.6 in $MgB_{2-x}Be_x$, Mg–Mg bond decreases from 3.084 to 3.062 Å, resulting in T_c depressing from 38.4 to 8.4 K [4]. Similarly, the T_c of C doped MgB_2 decreases by 17 K as the Mg–Mg bond contracts from 3.87 to 3.055 Å while the c-axis remains unchanged in $Mg(B_{0.8}C_{0.2})_2$ [5, 6]. It is of interest that superconductivity is retained in $Mg(B_{0.8}C_{0.2})_2$ when the Mg–Mg bond length is 3.055 Å, although this leads to the loss of superconductivity in the Al doped materials and the nano-crystalline MgB_2 of 2.5 nm. This may be due to the different nature of the replacements in Mg and B sites. The substitution of C for B changes the charge distribution of σ-bonding states in the B planes that couple very strongly to the in-plane vibration of B atoms. Therefore, such a substitution affects strong-electron-pair formation of the σ-bonding states, which are crucial to the appearance of superconductivtiy in MgB_2 [1, 12]. In this case, the individual contribution from

electronic effects may partially compensate the lattice effects on T_c to yield different results as compared to the Al doped and nano-crystalline MgB_2. Regardless of the doping mechanisms and the atomic replacements, the experiments show that T_c is depressed whenever the Mg–Mg bond contracts, indicating that (1) the superconductivity of MgB_2 is highly sensitive to lattice structure, (2) the Mg–Mg bond dominates the superconducting transition behaviour, and (3)
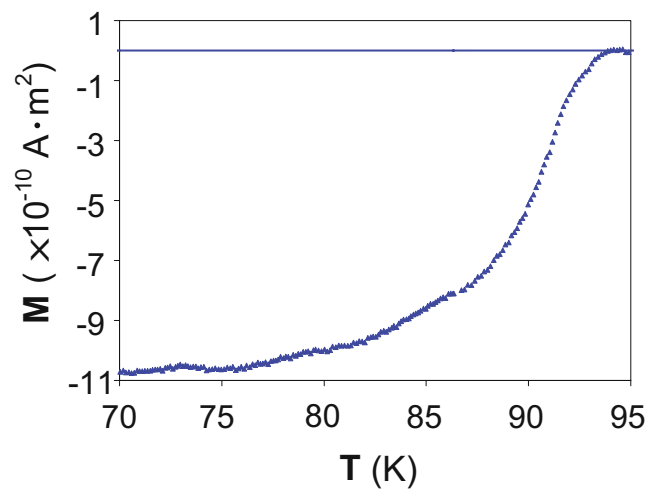
Fig. 4 Magnetic moments as a function of temperature shows that the nanocrystalline $YBa_2Cu_3O_{7-\delta}$ of 4 nm presents superconducting transition at 93 K, indicating this class of superconducting materials possess size independence of superconductivity

Table 2 Superconducting transition temperature and lattice parameters of $RBa_2Cu_3O_{7-\delta}$.

Compounds	YBa_2 Cu_3O_{7-x}	$NdBa_2$ Cu_3O_{7-x}	$DyBa_2$ Cu_3O_{7-x}	$EuBa_2$ Cu_3O_{7-x}	$GdBa_2$ Cu_3O_{7-x}	$HoBa_2$ Cu_3O_{7-x}	$ErBa_2$ Cu_3O_{7-x}	$TmBa_2$ Cu_3O_{7-x}
T_c(K)	91.5	92	91.2	93.7	92.2	92.2	91.5	91.2
a	3.817(1)	3.8595(1)	3.8284(8)	3.8407(1)	3.8416(4)	3.8193(1)	3.8156(1)	3.8090(1)
b	3.883(1)	3.9117(2)	3.8888(8)	3.9001(1)	3.8984(4)	3.8848(1)	3.8814(1)	3.8778(1)
c	11.633(1)	11.7449(5)	11.668(2)	11.720(2)	11.707(1)	11.6786(3)	11.6706(3)	11.6685(3)
Cell volume	172.42	177.32	173.71(5)	175.56	175.33	173.28	172.84	172.35

increasing T_c of MgB_2 may not be readily achieved by varying the Fermi-level density-of-states through chemical doping.

3.2 Lattice parameter independence of critical transition temperature in $YBa_2Cu_3O_{7-\delta}$

For comparison, the identical experiments above were carried on $YBa_2Cu_3O_{7-\delta}$ and the magnetic moments as a function of temperature for the as-prepared nano-crystalline $YBa_2Cu_3O_{7-\delta}$ of 4 nm is plotted in Fig. 4. The result shows that T_c of $YBa_2Cu_3O_{7-\delta}$ is entirely independence of the crystal size above ~4.0 nm but the superconductivity is lost spontaneously when the crystal size is smaller than this crystal size. It exhibits insensitivity to lattice parameters but the electron structure such as the concentration of doped oxygen. Although hydrostatic pressure was also used to investigate the lattice effects on T_c of $YBa_2Cu_3O_{7-\delta}$, showing that T_c increased as the crystal lattice got smaller by increasing the pressure, this result may not reflect the actual mechanism behind the T_c variation due to the change of equilibrium state caused by increasing pressure.

On both experimental and theoretical grounds, superconductivity and charge transport of high-T_c superconductors are mostly confined to the Cu–O planes. The T_c of these superconductors depends on the number of Cu–O layers in the unit cell. Two of CuO_2 planes, those through the interior of the cell in $YBa_2Cu_3O_{7-\delta}$, lead to T_c of 92 K. On the other hand, it has been proposed that the long-range ordering antiferromagnetic nature of the spin fluctuations is responsible for the high-T_c superconduc-

tivity in $YBa_2Cu_3O_{7-\delta}$ oxide [13]. The local 'striped' antiferromagnetic ordering was modulated with a period of eight lattice spacings [14]. It can be inferred that T_c might not changed with the variation of lattice parameters through the size reduction as long as the crystal size is greater than the minimum range of antiferromagnetic ordering essential for rendering $YBa_2Cu_3O_{7-\delta}$ superconducting. Furthermore, the compounds with full substitutions of Y by many rare earth elements in $RBa_2Cu_3O_{7-\delta}$ have similar T_c (Table 2) where R is rare earth elements that have different atomic size and physical properties but similar chemical properties. This supports the notion that $YBa_2Cu_3O_{7-\delta}$ may not be very sensitive to the lattice parameters in ambient pressure but extremely sensitive to the electron structure such as the concentration of oxygen.

3.3 Separating the lattice structural effect and electron contribution to band structure of ZnO

Because of the unique properties in photonic, piezoelectricity and microelectronics, the wide-gap semiconductor-ZnO has attracted enormous interests to develop this material for a number of electronic and photonic applications through doping technology. It is important to understand the individual effect from the variation of lattice and electron structures on ZnO band structure, thus indicating a direction to achieve the desired properties. Table 3 lists the size dependence of the lattice parameters, showing that the **a** and **c** axes increase as the crystal size decreases. Figure 5 plots the normalized emission intensity versus wavelength for the as-prepared nano-crystalline

Table 3 Size dependence of lattice parameters of ZnO.

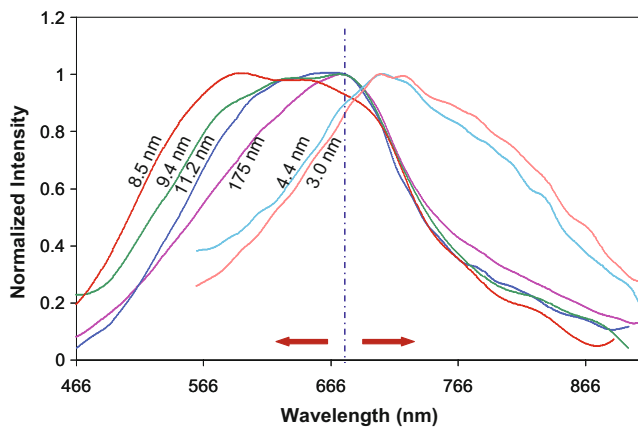| Crystal Size (nm)	175	11.2	9.4	8.5	4.4	3.0
a axis (Å)	3.2509	3.2498	3.2513	3.2533	3.256	3.2567
c axis (Å)	5.2054	5.2066	5.2077	5.2092	5.213	5.2122
Cell volume ($Å^3$)	47.6414	47.6208	47.6759	47.7472	47.8469	47.8757

Fig. 5 Normalized emission intensity versus emission wavelength shows the size dependence of band structures in ZnO

ZnO. The results exhibit that the emission profile has blue shifting as the crystal size is reduced from 202 to 8.5 nm while a red shifting is discernable when the crystal size is smaller than 8.5 nm. These indicate that the intrinsic structural behavior of nanocrystals may lead to the variation of physical properties and band structure in ZnO.

It is still not clear whether the change of lattice parameters caused by the size reduction would result in a change of Zn or oxygen occupancies in the lattice. But the variation of electron structure with the change of lattice parameters through the size reduction is discernable in the spectra of x-ray photoelectron spectroscopy (XPS) (Fig. 6). Although it is a bit difficult to separate the lattice effects from electron contribution to band structure with IPAN in this case, the individual effect of electron structure variation could be understood by deoxygenation experiment with minimum disruption in crystallographic system. Subtracting

the contribution from the lattice variation caused by the oxygen vacancies, the individual electronic structural contribution to the band structure could be clearly revealed and the results will be reported in future.

4 Conclusion

The individual effects of lattice and electron structures on critical transition temperatures of MgB_2 and $YBa_2Cu_3O_{7-\delta}$ have been experimentally separated by exploiting the nanosize dependence of lattice structure to modify the structural parameters without resorting to chemical doping. The results show that the T_c of MgB_2 is extremely sensitive to lattice parameter variation, such that contraction of Mg–Mg bond dramatically depresses T_c and eventually results in the loss of superconductivity as the average coordination of Mg to B falls from 12 to 8 due to the introduction of B vacancies for nano-crystalline MgB_2 of 2.5 nm in diameter. But the superconductivity of $YBa_2Cu_3O_{7-\delta}$ is more sensitive to the variation of electron structure and independent on the variation of lattice parameters as long as the crystal size is greater than the minimum range of antiferromagnetic ordering essential for rendering the superconductivity.

Although the effects of lattice parameters on band structure of ZnO is complex and the change of lattice parameters results in the variation of electron structure, the individual contributions from lattice and electron structures could be further separated by combining the IPAN technique and the deoxygenation experiment. The results in this work has successfully demonstrated that IPAN is an effective technique to understand the lattice structure and electron structure effects on the physical properties, thus providing new insight into fundamental mechanism of the dominant factors for the properties.

Fig. 6 XPS spectra of nano-crystalline ZnO with crystal size of (**a**) 202 and (**b**) 3 nm
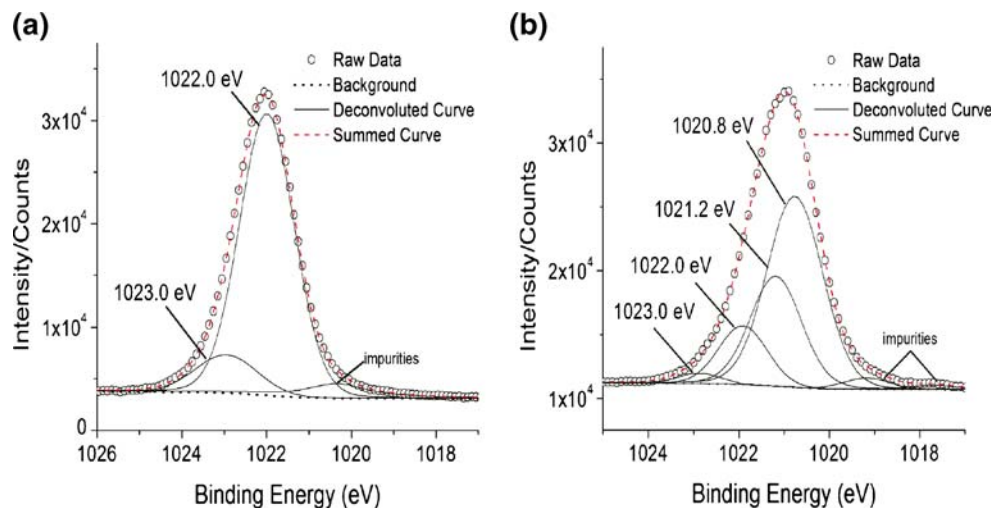
References

1. O. de la Peña, A. Aguayo, R. de Coss, Phys. Rev., B **66**, 012511 (2002)
2. Y.G. Zhao, X.P. Zhang, P.T. Qiao, H.T. Zhang, S.L. Jia, B.S. Cao, M.H. Zhu, Z.H. Han, X.L. Wang, B.L. Gu, Physica, C **361**, 91 (2001)
3. J.S. Ahn, E.S. Choi, W. Kang, D.J. Singh, M. Han, E.J. Choi, Phys. Rev., B **65**, 2145341 (2002)
4. W. Mickelson, J. Cumings, W.Q. Han, A. Zettl, Phys. Rev., B **65**, 052505 (2002)
5. R.A. Ribeiro, S.L. Bud'ko, C. Petrovic, P.C. Canfield, Physica, C **384**, 227 (2003)
6. J. Tang, L.C. Qin, A. Matsushita, Y. Takano, K. Togano, H. Kito, and H. Ihara, Phys. Rev., B **64**, 132509 (1999)
7. J.S. Slusky, N. Rogado, K.A. Regan, M.A. Hayward, P. Khalifah, T. He, K. Inumaru, S.M. Loureiro, M.K. Haas, H.W. Zandbergen, R.J. Cava, Nature **410**, 343 (2001)
8. K. Shimizu, T. Kimura, S. Furomoto, K. Takeda, K. Kontani, Y. Onuki, K. Amaya, Nature **412**, 316 (2001)
9. S.S. Saxena, P. Agarwal, K. Ahilan, F.M. Grosche, R.K.W. Haselwimmer, M.J. Steiner, E. Pugh, I.R. Walker, S.R. Julian, P. Monthoux, G.G. Lonzarich, A. Huxley, I. Sheikin, D. Braithwaite, J. Flouquet, Nature **406**, 587 (2000)
10. A. Vegas, Crystallogr. Rev. **7**, 189 (2000)
11. C.Q. Sun, W.H. Zhong, S. Li, B.K. Tay, H.L. Bai, E.Y. Jiang, J. Phys. Chem., B **108**, 1080 (2004)
12. S. Souma, Y. Machida, T. Sato, T. Takahashi, H. Matsui, S.C. Wang, H. Ding, A. Kaminski, J.C. Campuzano, S. Sasaki, K. Kadowaki, Nature **423**, 65 (2003)
13. J. Orenstein, A.J. Millis, Science **288**, 468 (2000)
14. B. Lake, H.M. Rønnow, N.B. Christensen, G. Aeppli, K. Lefmann, D.F. Mcmorrow, P. Vorderwisch, P. Smeibidl, N. Mangkorntong, T. Sasagawa, M. Nohara, H. Takagi, T.E. Mason, Nature **415**, 299 (2002)